Atmos. Chem. Phys. Discuss., 11, 26815–26848, 2011
www.atmos-chem-phys-discuss.net/11/26815/2011/
doi:10.5194/acpd-11-26815-2011

Atmospheric Chemistry and Physics Discussions

The adsorption of peroxynitric acid on ice between 230 K and 253 K

T. Ulrich[1,2], M. Ammann[1], S. Leutwyler[2], and T. Bartels-Rausch[1]

[1]Department of Biology and Chemistry, Paul Scherrer Institut, Villigen, Switzerland
[2]Department of Chemistry and Biochemistry, University of Berne, Berne, Switzerland

Received: 12 September 2011 – Accepted: 22 September 2011
– Published: 28 September 2011

Correspondence to: T. Bartels-Rausch (thorsten.bartels-rausch@psi.ch)

Published by Copernicus Publications on behalf of the European Geosciences Union.

Abstract

Peroxynitric acid uptake to ice and snow has been proposed to be a major loss process from the atmosphere with impacts on the atmospheric oxidation capacity. Here we present results from a laboratory study on the interaction of peroxynitric acid with water ice at low concentrations. Experiments were performed in a coated wall flow tube at atmospheric pressure and in the environmentally relevant temperature range of 230 K to 253 K. The interaction was found to be fully reversible and decomposition was not observed. Analysis based on the Langmuir adsorption model showed that the partitioning of peroxynitric acid to ice is orders of magnitude lower than of nitric acid and similar to nitrous acid partitioning behavior. The partition coefficient (K_{LinC}) and its temperature dependency can be described by $3.74\times10^{-12}\times e^{(7098/T)}$ [cm]. Atmospheric implications are discussed and show that the uptake to cirrus clouds or to snow-packs in polar areas is an important sink for peroxynitric acid in the environment.

1 Introduction

The nitrogen oxide peroxynitric acid (HO_2NO_2) is an atmospheric trace gas that interlinks both HO_x (= OH + HO_2) and NO_x (= NO + NO_2) chemistry. Connected with those trace gas families are the rate of ozone (O_3) production and also the oxidative capacity of the atmosphere. Because HO_2NO_2 is thermally unstable (Gierczak et al., 2005), HO_2NO_2 makes up a significant fraction of the total nitrogen oxide budget in the colder parts of the environment. Concentrations up to 1.6×10^{9} molecules cm^{-3} have been measured at South Pole (Slusher et al., 2002), up to 2.9×10^{10} molecules cm^{-3} above the Antarctic plateau (Slusher et al., 2010) and a mean of 5.7×10^{8} molecules cm^{-3} in the upper troposphere (Kim et al., 2007). The thermal lifetime of HO_2NO_2 is a strong function of temperature and is approximately a few seconds at 298 K, 10 h in the upper troposphere, and 2 h at South Pole. Currently, the fate of HO_2NO_2 in the atmosphere is not well enough known to be captured in atmospheric-chemistry mod-

ACPD
11, 26815–26848, 2011

els, which generally overestimate its gas-phase concentrations. The observed diurnal profiles of HO_2NO_2 at South Pole could only be explained when postulating a strong sink removing HO_2NO_2 from the gas-phase (Slusher et al., 2002). Deposition to snow has been proposed as such sink. Also, the observed decrease in gas-phase HO_x concentration at high NO_x levels was explained by the deposition of HO_2NO_2 to the snow (Chen et al., 2001; Grannas et al., 2007). In the upper troposphere, a HO_2NO_2 sink is also missing from the model descriptions; currently the observed altitude profiles cannot be reproduced. In their field study Kim et al. (2007) did not find a clear indication for reduced HO_2NO_2 gas-phase concentrations in ice clouds, but data is insufficient to draw sound conclusions, and uptake to ice particles in cirrus clouds remains one of several potential sink processes as the authors noted.

The choice to include a strong deposition of HO_2NO_2 to the snow or ice clouds was motivated by an earlier laboratory study that showed a strong irreversible uptake of HO_2NO_2 to ice (Li et al., 1996). In their study Li et al. (1996) derived a steady state uptake coefficient of 0.2 for HO_2NO_2 on ice. The uptake coefficient is defined as the net probability that a molecule that gas-kinetically collides with a surface is taken up at the surface. Values of 0.2 persisting over longer times indicate a strong uptake. A strong uptake over longer timescales has been recognized for acidic trace gases such as HNO_3 (Huthwelker et al., 2006; Ullerstam et al., 2005). The results of Li et al. (1996) are however not representative for HO_2NO_2 ice interactions, because the experiments have been performed at very high concentrations of HO_2NO_2. HO_2NO_2hydrates may form at such high HO_2NO_2 levels. Further, HNO_3 concentrations, a by-product of the HO_2NO_2 synthesis, were so high that the work was certainly done outside the ice stability regime of the HNO_3 –water phase diagram. Both might well explain the observed long lasting uptake. Uptake behavior to ice surfaces might therefore be distinctly different than observed by Li et al. (1996). The main aim of this study was thus to investigate the uptake of HO_2NO_2 to ice at low surface coverage of HO_2NO_2 and its by-products. Further the uptake of HO_2NO_2 to ice is compared with that of other trace gases and discussed, based on their solubility and acidity.

ACPD
11, 26815–26848, 2011

2 Methods

The interaction of HO_2NO_2 with a smooth water-ice film was studied in a coated wall flow tube (CWFT) at atmospheric pressure. The HO_2NO_2 was synthesized in the gas phase by reaction of NO_2 with HO_2 and monitored by means of a chemical ionization mass spectrometer (CIMS) situated after the CWFT. Figure 1 shows the setup of the experiments. Gases originate from certified gas bottles of N_2 (CarbaGas, 99.999 %), 20 % O_2 (CarbaGas, 99.995 %) in N_2 (CarbaGas, 99.999 %), 10 ppm NO (Messer, 99.8 %) in N_2 (Messer, 99.999 %) and 10 % CO (Messer, 99.997 %) in N_2 (Messer, 99.9999 %). Gas flows were controlled with calibrated mass flow controllers (Brooks 5850) or gas flow regulators (Voegtlin red-y) with better than 1 % accuracy. The flow through the CWFT was given by the size of the sampling orifice situated between the CWFT and the CIMS at low pressure. The volumetric gas flows were measured once a day with a gas flow calibrator (M-5 mini-Buck Calibrator, A.P. Buck Inc.) with 0.5 % accuracy. All flows in this work refer to standard pressure and temperature (1.013×10^5 Pa and 273.15 K). The entire flow system consisted of perfluoroalkoxy (PFA) tubing.

The synthesis has been described previously (Bartels-Rausch et al., 2011). First, NO_2 is quantitatively synthesized in a reactor of 2 L (RV 1, Fig. 1) by mixing a flow of 83 ml min^{-1} NO in N_2 with a flow of 700 ml min^{-1} N_2 and a small flow (around 6 ml min^{-1}) of O_3. O_3 is produced by irradiating dry synthetic air with 172 nm light (PhotRct 1, Fig. 1). Then HO_2NO_2 is produced by the reaction of NO_2 with HO_2, which is synthesized by photolysis of H_2O in presence of CO and O_2 also at 172 nm. NO_2 at typically 3.4×10^{12} molecules cm^{-3} initial concentration is also present for immediate reaction in the photolysis reactor (PhotRct 2, Fig. 1), where the synthesis took place. CO lowers the yield of HNO_3 and raises the yield of HO_2NO_2 as shown in Bartels-Rausch et al. (2011). In the photolysis reactor a flow of 700 ml min^{-1} N_2 was mixed with 2.5 ml min^{-1} CO and with 783 ml min^{-1} NO_2 in N_2. About half of the experiments were done at a higher CO flow of 10 ml min^{-1}. The residence time in the photolysis reactor was 270 ms. Humidity in the photolysis reactor was set to 10 %. The concen-

ACPD
11, 26815–26848, 2011

tration of the by-products HONO, HNO_3, and H_2O_2 in the gas flow was reduced by a Ti(IV) oxysulfate denuder and by a cooling trap at 243 K. The Ti(IV) oxysulfate denuder was prepared by wetting a 49 cm long sandblasted quartz glass tube with a diameter of 0.7 cm with a 5 % solution of Ti(IV) oxysulfate in 30 % H_2SO_4 (Fluka 89532) and drying the solution in a flow of nitrogen until a very concentrated and highly viscous solution was gained. The cooling trap consisted of a 46 cm long glass tube with an inner diameter of 2.4 cm that was filled with 10 ml quartz spheres to enhance surface area.

Following the synthesis and purification of HO_2NO_2 560 ml min^{-1} of the gas flow were fed into the CWFT after a dilution step with humidified N_2. The CWFT consisted of a quartz tube with an inner diameter of 0.8 cm and a length of 44 cm. To prepare the ice film, the quartz tube was etched on the inside with a 5 % solution of hydrofluoric acid (HF) in water, and then rinsed with ultra pure water (MilliQ water, 0.05 µS, pH: 7.3) until the pH was neutral. The pH was determined with a pH electrode optimized and calibrated for solutions of low ionic strength (Orion 3 Star, Thermo). The quartz tube was then held vertically for exactly 60 s, to let excess water flow out. An ice film was frozen at 258 K by rotating the quartz tube in a snuggly-fitting cooling jacket. This procedure results in smooth ice films, so that its surface area can be calculated based on its geometry (Abbatt, 2003; Huthwelker et al., 2006). The ice had a thickness of 10 µm ±2.7 µm as determined by weighing. Weighing was also used to check for eventual gain or loss of water during the CWFT experiment; gain was never observed, in most experiments a slight loss of 15 % (mean value) was observed. The cooling jacket was tempered with a circulating ethanol bath. Temperatures were measured with a Pt100 thermo-element directly inside the CWFT at experimental conditions. The temperature gradient along the length of the flow tube was very small. At 253 K the entrance of the CWFT was about 0.03 K warmer than temperatures at its end, and at 230 K the difference was about 0.2 K. At any position temperatures were very stable, the standard deviation at 230 K was ±0.05 K. For the HO_2NO_2 adsorption measurements, a gas flow of typically 560 ml min^{-1}, containing around 8.16×10^{10} molecules cm^{-3} HO_2NO_2 was passed over

ACPD
11, 26815–26848, 2011

the ice and its change in concentration with time was monitored in the gas-phase after the CWFT. Reynolds numbers with an average value of 112 indicate a laminar flow regime in the CWFT. To evaluate the desorption behavior of the adsorbed HO_2NO_2, the release of HO_2NO_2 from the ice surface was observed by passing HO_2NO_2 free carrier gas over the ice that was previously exposed to HO_2NO_2 until equilibrium was reached. This was achieved by selectively decomposing HO_2NO_2 to NO_2 and HO_2 in a heating system, consisting of a 2 m long PFA tube (I.D.: 4 mm) heated up to 373 K, in front of the CWFT. The residence time of the gas in the heating system was 730 ms. The advantage of this method is that exactly the same gas mixture is used with the same humidity, only without HO_2NO_2. The evolution of HO_2NO_2 in the gas-phase after contact with the ice was measured using a CIMS (Guimbaud et al., 2003). The CIMS is differentially pumped: ionization chamber (CI): 12 mbar, intermediate chamber (IC): 1.4×10^{-4} mbar and quadrupole and detection chamber (MS): 1.3×10^{-6} mbar. SF_6^- was used as ionization species. The CI had a total length of 16.5 cm and an I.D. of 17 mm. The flow in STP of around 560 ml min^{-1} exiting the HO_2NO_2 synthesis was mixed with 5 ml min^{-1} 1 % SF_6 (Messer, UHP) in Ar (Messer, 99.999 %) and 1200 ml min^{-1} N_2 (CarbaGas, 99.999 %). SF_6^- ions were produced by passing the SF_6 in N_2 mixture through a ^{210}Po-ionizer (NRD, p-2031). A negative voltage of 236 V was applied to the CI, while the orifice of the CIMS was held at −5 V. Several clusters, which have been described earlier, have been observed with the CIMS: SF_6^- the ionizing species at mass to charge ratio (m/z) 146, $SF_6^-(H_2O)$ its water cluster at *m/z* 164, $NO_4^-(HF)$ from HO_2NO_2 at *m/z* 98 (Slusher et al., 2001), $NO_3^-(HF)$ from HNO_3 at *m/z* 82 (Huey, 2007), $NO_2^-(HF)$ from HONO and HO_2NO_2 at *m/z* 66 (Longfellow et al., 1998), NO_2^- from NO_2 at *m/z* 46 (Huey, 2007) and $SF_4O_2^-$ from H_2O_2 at *m/z* 140 (Bartels-Rausch et al., 2011). The fragment with *m/z* 66 originates not only from HONO but also from HO_2NO_2. To derive HONO levels from the *m/z* 66 trace, the fraction of the $NO_2^-(HF)$ cluster originating from HO_2NO_2 was subtracted from total intensity. Stable humidity during the experiment, and in particular identical humidity in the carrier gas, whether or not it passed the ice in the CWFT, was ensured by monitoring the intensity of the

ACPD
11, 26815–26848, 2011

SF_6^- (H_2O) cluster at *m/z* of 164. We observed that this cluster responds strongly and reproducible to changes in relative humidity between 0.2 % and 10 %. For further analysis, the intensities of the individual traces were normalized to the intensity of SF_6^- trace. With this setup detection limits ($3\times\sigma$) for HO_2NO_2 of 2.3×10^8 molecules cm^{-3} in the chemical ionization chamber were reached. This corresponds to a concentration of 5.2×10^{10} molecules cm^{-3} in the CWFT, i.e. before dilution and pressure drop. To evaluate the performance of the Ti(IV) denuder and the cooling trap the concentrations of HO_2NO_2 and the by-products were quantified with individual experiments. The HONO concentration was quantified with a commercial HONO analyzer (LOPAP, QUMA (Heland et al., 2001; Kleffmann et al., 2002)). The H_2O_2 concentration was measured with a commercial H_2O_2 analyzer (AeroLaser AL 1002). NO_2, HNO_3 and HO_2NO_2 concentrations were quantified by a commercial NO_x analyzer (Monitor Labs 9841 A). This instrument measures NO directly by chemiluminescence, and NO_y (= NO + NO_2 + NO_3 + N_2O_4 + N_2O_5 + HONO + HNO_3 + HO_2NO_2 + PAN + other organic nitrates) after conversion to NO in a molybdenum converter. In this study NO could not be quantified, because the CO in the sample gas interfered with the NO detection. This interference was not observed when the CO was passed via the molybdenum converter. To differentiate between the individual NO_y species chemical traps were used (Ammann, 2001). A trap of Na_2CO_3 coated on firebricks, was used to scavenge all acidic nitrogen oxides that might be produced by the synthesis (HONO, HNO_3 and HO_2NO_2) and thus to differentiate between those and the remaining NO and NO_2 in the gas phase. Prior to its use the Na_2CO_3 was exposed to NO_2 in order to minimize the uptake of NO_2 that is otherwise observed during the experiments. Similarly a NaCl trap was used to differentiate between HNO_3 and the other NO_y species; it consisted of a sandblasted quartz tube with a length of 49 cm and an inner diameter of 0.8 cm, wetted inside with a slurry of NaCl in 1/1 water/methanol, and dried in a stream of N_2 (Ammann, 2001). To quantify HO_2NO_2 a heating trap was used to decompose HO_2NO_2 quantitatively to NO_2 in combination with the Na_2CO_3 trap to either scavenge HONO, HNO_3, and HO_2NO_2 or only HONO and HNO_3 (Bartels-Rausch et al., 2011). This measurement

ACPD
11, 26815–26848, 2011

was also used to calibrate the HO_2NO_2 trace of the CIMS for continuous quantification of HO_2NO_2 during each CWFT experiment.

3 Results and discussion

Conventionally HO_2NO_2 is synthesized in the aqueous phase by reaction of NO_2BF_4 in 90 % H_2O_2 or of $NaNO_2$ and $HClO_4$ in 30% H_2O_2, which is then delivered to a gas-flow by bubbling carrier gas through the solution (Kenley et al., 1981; Appelman and Gosztola, 1995). One advantage of the gas-phase synthesis used here is that it can continuously provide HO_2NO_2 levels over long time periods, as needed for our experiments. Also, the handling of concentrated, explosive H_2O_2 solutions is omitted. Niki et al. (1977) synthesized HO_2NO_2 in the gas-phase by photolysis of HCl and subsequent reaction of the produced HO_2 with NO_2. Here, we used a different approach where H_2O is photolyzed as the HO_2 source in order to eliminate HCl and ClONO and potential interference of these by-products with the adsorption experiments. We have shown previously that HO_2NO_2 yields of up to 30 % can be achieved with this synthesis route by adding CO to the photolysis gas mixture (Bartels-Rausch et al., 2011). The presence of CO shifts the OH to HO_2 equilibrium towards HO_2 (Reactions R3 and R4) (Aschmutat et al., 2001). HO_2NO_2 is then formed by the same reaction as in the atmosphere (Niki et al., 1977):

$$HO_2 + NO_2 + M \rightarrow HO_2NO_2 + M \quad \text{(R1)}$$

The hydrolysis of water at 172 nm in the presence of oxygen is the source of HO and HO_2 (Reactions R2 and R4).

$$H_2O + h\nu \rightarrow OH + H \quad \text{(R2)}$$

$$CO + OH \rightarrow CO_2 + H \quad \text{(R3)}$$

$$H + O_2 \rightarrow HO_2 \quad \text{(R4)}$$

ACPD
11, 26815–26848, 2011

The main problem associated with both, gas-phase and aqueous phase synthesis routes, is the presence of by-products. In our previous study we identified HNO_3 with a yield of 30% and HONO with a yield of 10 % (Bartels-Rausch et al., 2011). HNO_3 is formed by reaction of NO_2 with OH (Reaction R5). In the absence of CO, this reaction has been used previously as a gas-phase source of HNO_3 with yields of up to 70 % (Vlasenko et al., 2009). HONO is the product of the OH + NO Reaction (R6), where NO is presumably formed by reaction of NO_2 with H or O radicals.

$$NO_2 + OH \rightarrow HNO_3 \quad \text{(R5)}$$

$$NO + OH \rightarrow HONO \quad \text{(R6)}$$

Another, major by-product – that has not been previously analyzed – might be H_2O_2, which is formed by the HO_2 self-reaction (Reaction R7).

$$HO_2 + HO_2 \rightarrow H_2O_2 + O_2 \quad \text{(R7)}$$

3.1 Purification of the synthesis from by-products

For this study the HO_2NO_2 synthesis was significantly improved by adding a Ti(IV) denuder to remove H_2O_2. HNO_3 was scrubbed from the gas phase in a cooling trap. Figure 2 shows the performance of the two purification steps for a typical experimental run. The data were obtained at initial concentrations of 3.4×10^{12} molecules cm^{-3} NO_2, 5.4×10^{15} molecules cm^{-3} O_2, 1.6×10^{16} molecules cm^{-3} CO, and 2.36×10^{18} molecules cm^{-3} water vapor. We found that the Ti(IV) denuder leads to a significant decrease of H_2O_2 by 99 % (Fig. 2, 235 min–295 min). Ti(VI) oxysulphate reacts quantitatively and fast with H_2O_2 to form $[Ti(O_2)(OH)_{aq}]^+$ complexes. This has previously been used as an analytical method (Possanzini et al., 1988). Also HONO was reduced by 94 % and 55 % of the HO_2NO_2 is trapped by the denuder, which lowers the overall yield of the synthesis route substantially. The increase of NO_2 and strong rise in HNO_3 of 15 % and 240 %, respectively,

ACPD
11, 26815–26848, 2011

indicate that these species were produced by redox processes in the Ti(IV) denuder system. The subsequently installed cooling trap reduces the HNO_3 by 86 % of its concentration after the Ti(IV) denuder (Fig. 3 235–267 min). The remaining concentration of HNO_3 was 20 % of the HO_2NO_2 concentration, which is comparable to or lower than that reported for the two synthesis routes in the aqueous phase (Jimenez et al., 2004; Knight et al., 2002). Knight et al. (2002) measured a HNO_3 concentration of around 10 % of the HO_2NO_2 in his sample at 273 K. Jimenez et al. (2004) measured a HNO_3 concentration of around 50 % of the HO_2NO_2 concentration behind a cold trap at 252 K. Considering H_2O_2, Knight et al. (2002) measured H_2O_2 concentrations of around 50 % and Jimenez et al. (2004) of about 10 % of the HO_2NO_2 concentration both of which is substantially lower than achieved here, even with the very efficient Ti-denuder. In our experiments the H_2O_2 concentration was still twice as that of HO_2NO_2. Without purification HNO_3 levels stayed well below 10 % of the HO_2NO_2 concentration (Fig. 2, 310 min–330 min), i.e. the HNO_3 concentration could be substantially reduced without the use of the Ti(IV) denuder at the expense of more H_2O_2. The HNO_3 and HONO levels reported here prior to the purification are significantly lower than observed in our previous study (Bartels-Rausch et al., 2011) and HO_2NO_2 level is higher. Reasons for this might be the increased flow velocity through the photo reactor, or differences in the detection mode of HNO_3 and HONO, which were measured using very selective methods in this work.

In summary, this synthesis resulted in a reproducible concentration of HO_2NO_2 in the flow tube of $1.2\times10^{11}\pm2.2\times10^{10}$ molecules cm^{-3} at a CO concentration of 1.6×10^{16} molecules cm^{-3}. For about half of the experiments the CO concentration was lowered to 0.4×10^{16} molecules cm^{-3} that – in qualitative agreement with our previous study – resulted in lower yields of HO_2NO_2 and higher levels of HNO_3. For these experiments a mean HO_2NO_2 concentration of $0.8\times10^{11}\pm1.7\times10^{10}$ molecules cm^{-3} was determined.

ACPD
11, 26815–26848, 2011

3.2 Adsorption experiments

Figure 3 shows typical evolutions of the HO_2NO_2 concentration with time at different temperatures as measured at the end of the CWFT. Such measurements are referred to as breakthrough curves. At time = 0 s, the gas flow containing the HO_2NO_2 was passed over the ice film, and its intensity drops to the background level. Before the exposure to ice, stable levels of HO_2NO_2 in the gas flow were observed and for the analysis HO_2NO_2 was normalized to the average of its level between −50 s and 0 s. Then, within 200 seconds at our experimental conditions, the gas-phase concentration of HO_2NO_2 starts to recover. The onset of the recovery shows temperature dependence with a longer lag-time at lower temperatures. The time needed to reach full recovery depends strongly on temperature as expected for an adsorption process. The number of adsorbed HO_2NO_2 molecules in equilibrium is the primary observable of these experiments and is directly derived from the breakthrough curve. The area enclosed by the breakthrough curves is a direct measure of the number of HO_2NO_2 molecules adsorbed (n_{ads}) by the ice film until equilibrium over the entire length of the CWFT is reached. The number of adsorbed molecules (n_{ads}) is given by

$$n_{ads} = F(T) \cdot \text{Int\_Area} \cdot \frac{p_{HO_2NO_2} \cdot N_a}{R \cdot T} \quad (1)$$

where $F(T)$ is the volumetric velocity of the gas flow in $cm^3\,s^{-1}$ at the temperature of the CWFT, Int_Area is the integrated area of the curve in s, corrected for the time an inert trace gas would take to pass the CWFT, $p_{HO_2NO_2}$ is the partial pressure of HO_2NO_2 [MPa], N_a is the Avogadro constant [molecules mol^{-1}], R is the universal gas constant [$J\,mol^{-1}\,K^{-1}$] and T is the temperature [K]. The surface concentration of adsorbed HO_2NO_2 molecules at our experimental conditions ranged from $4.2\times10^{11}\pm2.1\times10^{11}$ molecules cm^{-2} at 253 K to $7.8\times10^{12}\pm3.9\times10^{12}$ molecules cm^{-2} HO_2NO_2 at 230 K, thus at most a few percent of a monolayer. The error estimates are based on the standard deviation of five repeated experiments at 230 K.

ACPD
11, 26815–26848, 2011

The HO_2NO_2 gas-phase concentration recovered to its initial level in all experiments. Incomplete recovery would suggest (i) chemical decomposition, (ii) slow, continuous uptake, or (iii) irreversible adsorption of HO_2NO_2. (i) Decomposition of HO_2NO_2 has been observed in water at moderate and acidic pH (Kenley et al., 1981; Lammel et al., 1990; Regimbal and Mozurkewich, 1997). HNO_3, NO_2, HONO, and H_2O_2 have been identified as products. On ice, Li et al. (1996) detected HNO_3 emissions from ice exposed to HO_2NO_2 but attributed those to impurities in the HO_2NO_2 source, and thus also concluded that HO_2NO_2 does not decompose on the ice surface. In our experimental setup, we would not expect to observe HNO_3 emissions from the ice, because of its strong tendency to stick to the ice surface. The CIMS traces of NO_2 at *m*/*z* 46 and of HONO at *m*/*z* 66 (corrected for intensity originating from HO_2NO_2) showed no increase when HO_2NO_2 was exposed to the ice surface, which further underlines our conclusion. (ii) HO_2NO_2 clearly does not show a long-term uptake as the HO_2NO_2 signal recovered completely within less than 20 minutes at our experimental conditions. The observation of a strong uptake over long timescales on thin ice films is restricted to highly acidic trace gases. Typical examples are HNO_3, HCl, and trifluoracetic acid (CF_3COOH) (McNeill et al., 2006; Ullerstam et al., 2005). Weaker acids, such as HO_2NO_2, show a fast and complete recovery. Analogous examples are formic acid (Symington et al., 2010; von Hessberg et al., 2008), acetic acid (Kerbrat et al., 2010a; Symington et al., 2010; von Hessberg et al., 2008), HONO (Chu et al., 2000), and SO_2 (Clegg and Abbatt, 2001). The non-acidic H_2O_2 shows no long term uptake (Clegg and Abbatt, 2001; Pouvesle et al., 2010). Table 1 lists the acidity and the molecular Henry coefficients (H_{298}) for different trace gases and shows that the observed complete recovery of HO_2NO_2 fully fits into the emerging picture where acidity largely determines the tendency for long-term uptake. Molecular solubility seems to be of minor importance. Instrumental fluctuations of ±10 % however give the possibility that small deviations from the complete recovery remained undetected. For the weak acids HONO and SO_2 a long term uptake has been observed in a packed bed flow tubes that have a much larger ice volume and surface area and are thus much

ACPD
11, 26815–26848, 2011

more sensitive to slow bulk and surface effects (Kerbat et al., 2010b; Huthwelker et al., 2001). (iii) To further test the reversibility of the uptake, the number of desorbing molecules was determined in 4 experiments at 230, 236.1, 238.3 and 244.1 K, respectively. For the individual experiments below 240 K the number of adsorbed and desorbed molecules was equal within the uncertainty of the measurements (±50 %) indicating fully reversible uptake. At 244.1 K the number of desorbed molecules was lower than the number of adsorbed molecules. This might be due to altered surface characteristics of the ice at higher temperatures. The observation of reversible adsorption is in agreement with other data available for weak acids or non-acidic species such as H_2O_2 (Pouvesle et al., 2010), acetone (Bartels-Rausch et al., 2004), formic acid (von Hessberg et al., 2008) and acetic acid (Sokolov and Abbatt, 2002; Symington et al., 2010). For the strong acids HNO_3 (Ullerstam et al., 2005) and HCl (McNeill et al., 2006) the peak area was significantly lower in the desorption experiments.

3.3 Partition coefficient

In summary, the uptake of HO_2NO_2 to the ice surface can be described as reversible adsorption equilibrium at temperatures below 240 K. To compare the adsorption behavior among different trace gases, we express the adsorption equilibrium in terms of the partition coefficient K_{LinC} (cm), which is defined as ratio of the concentration of adsorbed molecules to the gas-phase concentration at equilibrium and describes the initial linear part of an adsorption isotherm as defined by the Langmuir model. At equilibrium the surface concentration of adsorbates is related to the gas-phase concentration as:

$$K_{\mathrm{LinC}} = \frac{\frac{n_{\mathrm{ads}}}{A}}{\frac{n_{\mathrm{gas}}}{V}}, \tag{2}$$

where n_{gas} is the number of molecules in the gas phase [molecules], V the volume of the flow tube [cm^3] and A the geometric surface area of the ice film [cm^2]. The Langmuir

ACPD
11, 26815–26848, 2011

model has proven to describe the partitioning of a number of atmospheric trace gases well, including HNO_3 at low coverage (Ullerstam et al., 2005), HONO (Kerbrat et al., 2010b) and VOCs (Sokolov and Abbatt, 2002) and has also been adopted by IUPAC (Crowley et al., 2010). The temperature dependent K_{LinC} also allows extrapolation of our findings to different temperatures.

Figure 4 shows $\ln(K_{LinC})$ of HO_2NO_2 between ice and air, plotted versus the inverse temperature over the range $T = 230–253$ K. K_{LinC} at 230 K is 91.2 ±15.7 cm and decreases to 6.0 ±0.4 cm at 253 K. The data follow a linear trend, clearly showing that reversible partitioning describes the interaction of HO_2NO_2 with the ice surface very well. The single measurement of desorbing HO_2NO_2 at 244.1 K seems thus to be an outlier. The linear fit of $\ln(K_{LinC})$ vs. 1/T allows to describe the temperature dependency of K_{LinC} as $3.74\times10^{-12}\times e^{(7098/T)}$; the uncertainty of the exponent is ±661 K. The values of K_{LinC} and their uncertainty are independent the concentration of HO_2NO_2. Such a negative and Arrhenius type temperature dependency is in agreement with other trace gases that physically adsorb on ice (Huthwelker et al., 2006). Figure 4 also shows that K_{LinC} of HO_2NO_2 is nearly three orders of magnitude lower than the K_{LinC} of HNO_3 and lies in the same range as the K_{LinC} of HONO over the temperature range investigated. This means that at equilibrium HO_2NO_2 adsorbs less to ice than HNO_3 and about as much as HONO. Both K_{LinC} values were taken from the recent IUPAC compilation (Crowley et al., 2010) and are based on data from (Abbatt, 1997; Chu et al., 2000; Cox et al., 2005; Hynes et al., 2002; Kerbrat et al., 2010b; Ullerstam et al., 2005). This relative adsorption strength is in agreement with our previous study, where the migration of HO_2NO_2, HNO_3, HONO, and NO_2 was investigated in a packed ice bed flow tube along which temperature decreased with distance (Bartels-Rausch et al., 2011). Those experiments showed an increasing preference for the ice phase in the sequence $NO_2 <$HONO $= HO_2NO_2 <HNO_3$. It is also in agreement with Li et al. (1996) who observed that HNO_3 desorbs at higher temperatures (+25 K) than HO_2NO_2 in temperature programmed desorption experiments. This relative order of K_{LinC} deviates somehow from the sequence of solubility in liquid water where HNO_3 is much more

ACPD
11, 26815–26848, 2011

soluble than HO_2NO_2 and HO_2NO_2 is better soluble than HONO. The (effective) solubility of the these three acidic nitrogen oxides was derived from the molecular Henry constant (H_{298}) and the acidity, as listed in Table 1, in the pH range 5 to 9. Based on a broader comparison with a larger number of trace gases, an apparent correlation between the partitioning to ice, the acidity constant, and the molecular Henry constant is evident. Figure 5 shows the results of such a multiple linear regression for SO_2, HCOOH, CH_3COOH, CF_3COOH, HONO, HNO_3, HO_2NO_2, HCl and H_2O_2. The correlation is rather good when considering the large errors that might be associated with the three input parameters. Especially, the reported values of H_{298} for HO_2NO_2 might be overestimated as HO_2NO_2 easily decomposes in water, which makes reliable measurement of its H_{298} difficult.

The good correlation illustrates the importance of both the acidity and the solubility on the partitioning to ice. Apparently similar molecular properties determine the tendency for uptake into water and the adsorption on ice for these acidic trace gases. This even holds for organic trace gases. Sokolov et al. (2002) have found a poor correlation for a number of organic trace gases between H_{298} and K_{LinC} and argued that this indicates that complete solvation of the adsorbing trace gas does not occur. The difference in both studies is mainly, that we focused on acidic trace gases here, while Sokolov et al. (2002) studied mostly non-acidic, polar organics and the results indicate that acidic trace gases form of a hydrate shell upon adsorption – similar to the solvation process. The relationship found is given in Eq. (3) and can be used to roughly estimate the partitioning of any acidic trace gas to ice – as long as the pH of the ice allows for significant dissociation:

$$\log(K_{LinC}) = 0.4977 \cdot \log(H_{298}) - 0.1282 \cdot pK_a + 1.1362 \quad (3)$$

3.4 Enthalpy of adsorption

The slope of the linear fits to the data in the $\ln(K_{LinC})$ versus the inverse temperature plot (Fig. 4) is similar for HNO_3 and HONO and steeper for HO_2NO_2. This impression is

ACPD
11, 26815–26848, 2011

confirmed by a statistical F-test, that compares the slopes of the regressions in a pairwise manner, based on the uncertainties of each, where slope and uncertainty were derived from the IUPAC recommendation for the respective species (Crowley et al., 2010): While the slopes of the HNO_3-HONO pair and the HNO_3-HO_2NO_2 pair could not be shown to be different, which might be due to the large error of the temperature dependence of the K_{LinC} values for HNO_3, the slope of the HONO-HO_2NO_2 pair were statistically different with a confidence of 95 %. From the slope the standard enthalpy of adsorption (ΔH^0_{ads}) of $-59.0^{+5.5}_{-8.6}$ kJ mol^{-1} can be derived for HO_2NO_2. The uncertainties are given by the 95% confidence interval of the fit and by the effect that competitive Langmuir adsorption with H_2O_2 might have on the slope in Fig. 4 (see below). The later is temperature dependent which explains the asymmetric uncertainty bonds. When comparing ΔH^0_{ads} with literature values for other nitrogen oxides as given in Table 1, one obtains the sequence $NO < NO_2 < HONO = HNO_3 < HO_2NO_2$ except from a very high enthalpy of adsorption for HNO_3 reported by Thibert and Dominé (1998) of -68 ± 8.9 kJ mol^{-1}. The higher enthalpy of adsorption of HO_2NO_2 as compared to the other nitrogen oxides is a sign for stronger molecule-ice interactions of HO_2NO_2.

4 Effect of by-products

Despite careful purification steps, the possibility that remaining H_2O_2, HNO_3, HONO, and NO_2 impurities interfere with the adsorption measurements of HO_2NO_2 remains and is discussed in the following. NO_2 does not interact with the ice at temperatures of our experiment (Bartels-Rausch et al., 2002), thus its presence does not influence the adsorption measurements of HO_2NO_2. Dimerization of NO_2 to N_2O_4 is unlikely at these low concentrations and is thus neglected. HONO does adsorb to the ice, but since its concentration is only 1 % of HO_2NO_2 its contribution can be neglected. HNO_3 and H_2O_2 are present at relatively high concentration and both partition strongly to ice surfaces. We monitored their gas phase concentration by the mass spectrometer during each experiment. In all experiments the HNO_3 signal remained at background,

ACPD
11, 26815–26848, 2011

while for H_2O_2 the onset of the recovery of the signal is only visible in some very long experiments. This observation strongly suggests larger partitioning of either species to ice compared to HO_2NO_2, which – as a side note – strengthens the recent work on H_2O_2 adsorption to ice by Pouvesle et al. (2010) rather than the work by Clegg and Abbatt (2001). Using the K_{LinC} temperature relationship recommended by IUPAC for HNO_3 (Crowley et al., 2010) and by Pouvesle et al. (2010) for H_2O_2, the length of the CWFT along which both species are present during the time of the experiments can be estimated. HNO_3 completely adsorbs within less than 2 cm of the flow tube at any temperature and its influence on the partitioning of HO_2NO_2 to the ice in equilibrium over the whole length of the CWFT is thus neglected. H_2O_2 adsorbs along a length of up to 30 cm with a surface coverage ranging from 5 % to 10 % for temperatures between 253 K and 238 K, and from 10 % to 18 % below 238 K. At such low surface coverage, the interaction of HO_2NO_2 with ice is not influenced. To confirm this, we calculated the reduction in the number of adsorbed HO_2NO_2 molecules when H_2O_2 is present due to competition for adsorption sites, using the competitive Langmuir model as detailed in (Kerbrat et al., 2010a). The model did show that the surface concentration of HO_2NO_2 on the ice is lowered by 22 % at 228 K, by 11 % at 238 K and by 5 % at 250 K in presence of H_2O_2. This reduced uptake slightly reduces the derived values of K_{LinC}. As this effect is well within the experimental uncertainty of K_{LinC}, we neglected the influence of competitive adsorption.

All experiments were done in the ice stability regime of the HNO_3 – water phase diagram (Thibert and Dominé, 1998), and the H_2O_2 – water phase diagram (Foley and Giguere, 1951). Considering the first 2 cm of the CWFT, surface modification of the ice by HNO_3 could be important. McNeill (2006) have observed increased adsorption of acetic acid to ice when another strong acid, HCl, was dosed to the surface at a concentration that induced modifications to the surface as observed by ellipsometry. McNeill (2006) observed this increased adsorption at HCl concentrations near the boundary of the solid ice stability regime of the HCl-water phase diagram. For partial pressures corresponding more to the center of the ice stability regime in the phase diagram no

ACPD
11, 26815–26848, 2011

surface modification and no increased uptake of acetic acid was observed. The HNO_3 concentration in this study was rather in the middle of the solid ice stability regime of the HNO_3-water phase diagram, making it unlikely that surface modifications might have occurred, which enhance the uptake of HO_2NO_2. In agreement solid ice was still observed at upper 1.1 nm of the ice surface in presence of nitrate at concentrations similar to this study (Krepelova et al., 2010).

5 Atmospheric implications

Ice surfaces have been proposed to represent a sink for gas phase HO_2NO_2 (Kim et al., 2007; Slusher et al., 2002), and the magnitude of the uptake of HO_2NO_2 to ice surfaces has been proposed to be similar to that of HNO_3 (Slusher et al., 2002). In this study we could show that equilibrium partitioning of HO_2NO_2 to the ice surface at low concentration is orders of magnitude lower than expected purely based on its molecular solubility and propose the use of K_{LinC} to estimate the partitioning of a trace gases between ice surface and gas phase. Molecular Henry constants have been used to estimate the gas phase concentration of HO_2NO_2 over ice surfaces (Abida et al., 2011). With the results presented in this study, HO_2NO_2 would be detected, even at temperatures where HNO_3 stays on the ice surface. Here we discuss the equilibrium partitioning of HO_2NO_2 to ice clouds in the upper troposphere and to surface snow-pack under environmentally relevant conditions once the adsorption equilibrium is reached.

Figure 6 shows the fraction of HO_2NO_2 adsorbed to the ice phase in typical cirrus clouds in the upper troposphere. Typical temperatures and surface area densities of dense cirrus clouds, 3×10^{-4} to $10^{-5}\,\mathrm{cm}^2$ ice surface per cm^3 of free gas phase, were taken from observations (Popp et al., 2004). The fraction of the adsorbed species was calculated with the following equation proposed by Pouvesle et al. (2010):

$$\alpha = \frac{K_{\mathrm{LinC}}\cdot \mathrm{SAD}}{K_{\mathrm{LinC}}\cdot \mathrm{SAD}+1}, \tag{4}$$

ACPD
11, 26815–26848, 2011

where α [–] is the adsorbed fraction, K_{LinC} [cm] the partition coefficient as a function of the temperature and SAD [cm^{-1}] is the ice surface area per volume of gas phase (surface area density). The adsorption of HO_2NO_2 to the ice particles is only significant at cold temperatures (<210 K) and very dense cirrus clouds (3×10^{-4} cm^{-1}); then up to 70 % of the total HO_2NO_2 is trapped. Thus – when very dense clouds are present – the equilibrium partitioning of HO_2NO_2 to cirrus clouds could explain the discrepancy between measured and modeled data for HO_2NO_2 in the upper troposphere. That Kim et al. (2007) did not observe a drop of gas-phase HO_2NO_2 in the presence of cirrus clouds, was possibly because the clouds were simply not dense enough. Considering the snow cover on the ground, the surface to air-volume ratio is orders of magnitude higher than in clouds and HO_2NO_2 adsorbs almost completely to the ice phase in the interstitial air in snow even at warmer temperatures. Specific surface area of snow ranges from 20 cm^2 g^{-1} to >1000 cm^2 g^{-1} for melt-freeze crust and fresh dentritic snow, respectively. The density, and connected with that solid to air volume ratio, ranges from 0.1 g cm^{-3} to 0.6 g cm^{-3} for fresh and wind-packed snow, respectively (Dominé et al., 2008). The resulting surface area densities are in the range of 10's to 100's cm^{-1}. This extensive partitioning to the ice phase directly influences the transport of HO_2NO_2 through a snow-pack by diffusion. The diffusivity of species with a strong tendency to stick to ice surfaces, i.e. large K_{LinC}, is attenuated by a factor $1/f$ [–] (Eq. 8) (Dominé et al., 2008).

$$f_{HO_2NO_2} = \frac{1}{1 + SAD \cdot K_{LinC,HO_2NO_2}}, \tag{5}$$

where SAD is the surface area density [cm^{-1}]. Figure 7 shows f versus the temperature typical for snow-covered environments for a range of surface area densities, where the high SAD value represents fresh dendritic snow and the low value wind packed snow. At temperatures below 240 K diffusion is slowed more than a hundred times due to the interaction with the ice surface for any given snow-pack. Note that also the geometric properties of the snow-pack impact diffusion in snow.

ACPD
11, 26815–26848, 2011

In summary snow and ice particles represent a sink for HO_2NO_2 in the environment. Snow surfaces represent a sink at any typical temperature; adsorption of HO_2NO_2 on atmospheric ice particles strongly depends on the density of the ice clouds and temperature. The pH at the surfaces will further impact the adsorption processes.

6 Conclusions

The adsorption of HO_2NO_2 on ice and its temperature dependence has been characterized at low surface coverage. At our experimental conditions, uptake of HO_2NO_2 to ice is fully reversible and a slow, long-term loss to the ice was not observed. The partition constant K_{LinC} with a negative temperature dependence of $3.74\times10^{-12}\times e^{(7098/T)}$ (cm) was derived. Partitioning to ice of HO_2NO_2 is orders of magnitude smaller than values for HNO_3, and in the same range as values reported for HONO. Acidity and solubility of the trace gas could be shown to have an important impact on the adsorption behavior. Cirrus clouds in the upper troposphere and ice and snow surfaces at South Pole and other very cold parts of the environment are sink for gas-phase HO_2NO_2.

Acknowledgements. We gratefully thank M. Birrer for excellent technical support. We thank Josef Dommen and Peter Mertes for providing and help with the H_2O_2 analyzer. We also thank Yulia Sosedova for help with the HONO analyzer. We appreciate funding by the Swiss National Science Foundation, grant number 200021_121857.

ACPD
11, 26815–26848, 2011

References

Abbatt, J. P. D.: Interaction of HNO_3 with water-ice surfaces at temperatures of the free troposphere, Geophys. Res. Lett., 24, 1479–1482, doi:10.1029/97GL01403, 1997.

Abbatt, J. P. D.: Interactions of atmospheric trace gases with ice surfaces: Adsorption and reaction, Chem. Rev., 103, 4783–4800, doi:10.1021/cr0206418, 2003.

Abida, O., Mielke, L. H., and Osthoff, H. D.: Observation of gas-phase peroxynitrous and peroxynitric acid during the photolysis of nitrate in acidified frozen solutions, Chem. Phys. Lett., 511, 187–192, doi:10.1016/j.cplett.2011.06.055, 2011.

Amels, P., Elias, H., Götz, U., Steingens, U., and Wannowius, K. J.: Chapter 3.1: Kinetic investigation of the stability of peroxonitric acid and of its reaction with sulfur(IV) in aqueous solution, edited by: Warneck, P., Springer Verlag, Berlin, Germany, 77–88 pp., 1996.

Ammann, M.: Using N-13 as tracer in heterogeneous atmospheric chemistry experiments, Radiochim. Acta, 89, 831–838, doi:10.1524/ract.2001.89.11-12.831, 2001.

Appelman, E. H. and Gosztola, D. J.: Aqueous peroxynitric acid ($HOONO_2$) – a novel synthesis and some chemical and spectroscopic properties, Inorg. Chem., 34, 787–791, doi:10.1021/ic00108a007, 1995.

Aschmutat, U., Hessling, M., Holland, F., and Hofzumahaus, A.: A tunable source of hydroxyl (OH) and hydroperoxy (HO_2) radicals: in the range between 106 and 109 cm^{-3}, Institut für Atmosphärische Chemie, Forschungszentrum Jülich, Jülich, 811–816, 2001.

Bartels-Rausch, T., Eichler, B., Zimmermann, P., Gäggeler, H. W., and Ammann, M.: The adsorption enthalpy of nitrogen oxides on crystalline ice, Atmos. Chem. Phys., 2, 235–247, doi:10.5194/acp-2-235-2002, 2002.

Bartels-Rausch, T., Guimbaud, C., Gäggeler, H. W., and Ammann, M.: The partitioning of acetone to different types of ice and snow between 198 and 223 K, Geophys. Res. Lett., 31, L16110, doi:10.1029/2004GL020070, 2004.

Bartels-Rausch, T., Ulrich, T., Huthwelker, T., and Ammann, M.: A novel synthesis of the radiactively labelled atmospheric trace gas peroxynitirc acid, Radiochim. Acta, 99, 1–8, doi:10.1524/ract.2011.1830, 2011.

Becker, K. H., Kleffmann, J., Kurtenbach, R., and Wiesen, P.: Solubility of nitrous acid (HONO) in sulfuric acid solutions, J. Phys. Chem.-US, 100, 14984–14990, doi:10.1021/jp961140, 1996.

Bowden, D. J., Clegg, S. L., and Brimblecombe, P.: The Henry's law constant of trifluoroacetic

ACPD
11, 26815–26848, 2011

acid and its partitioning into liquid water in the atmosphere, Chemosphere, 32, 405–420, doi:10.1016/0045-6535(95)00330-4, 1996.

Chameides, W. L.: The photochemistry of a remote marine stratiform cloud, J. Geophys. Res.-Atmos., 89, 4739–4755, doi:10.1029/JD090iD03p05865, 1984.

Chen, C. C., Britt, H. I., Boston, J. F., and Evans, L. B.: Extension and Application of the Pitzer Equation for Vapor-Liquid-Equilibrium of Aqueous-Electrolyte Systems with Molecular Solutes, Aiche J., 25, 820–831, doi:10.1002/aic.690250510, 1979.

Chen, G., Davis, D., Crawford, J., Nowak, J. B., Eisele, F., Mauldin, R. L., Tanner, D., Buhr, M., Shetter, R., Lefer, B., Arimoto, R., Hogan, A., and Blake, D.: An investigation of South Pole HOx chemistry: Comparison of model results with ISCAT observations, Geophys. Res. Lett., 28, 3633–3636, 10.1029/2001GL013158, 2001.

Chu, L., Diao, G. W., and Chu, L. T.: Heterogeneous interaction and reaction of HONO on ice films between 173 and 230 K, J. Phys. Chem. A, 104, 3150–3158, 10.1021/jp9937151, 2000.

Clegg, S. M. and Abbatt, J. P. D.: Uptake of gas-phase SO_2 and H_2O_2 by ice surfaces: Dependence on partial pressure, temperature, and surface acidity, J. Phys. Chem. A, 105, 6630–6636, doi:10.1021/jp010062r, 2001.

Cox, R. A., Fernandez, M. A., Symington, A., Ullerstam, M., and Abbatt, J. P. D.: A kinetic model for uptake of HNO_3 and HCl on ice in a coated wall flow system, Phys. Chem. Chem. Phys., 7, 3434–3442, doi:10.1039/b506683b, 2005.

Crowley, J. N., Ammann, M., Cox, R. A., Hynes, R. G., Jenkin, M. E., Mellouki, A., Rossi, M. J., Troe, J., and Wallington, T. J.: Evaluated kinetic and photochemical data for atmospheric chemistry: Volume V – heterogeneous reactions on solid substrates, Atmos. Chem. Phys., 10, 9059–9223, doi:10.5194/acp-10-9059-2010, 2010.

Dominé, F., Albert, M., Huthwelker, T., Jacobi, H. W., Kokhanovsky, A. A., Lehning, M., Picard, G., and Simpson, W. R.: Snow physics as relevant to snow photochemistry, Atmos. Chem. Phys., 8, 171–208, doi:10.5194/acp-8-171-2008, 2008.

Durham, J. L., Overton, J. H., and Aneja, V. P.: Influence of gaseous nitric-acid on sulfate production and acidity in rain, Atmos. Envrion., 15, 1059–1068, doi:10.1016/0004-6981(81)90106-2, 1981.

Foley, W. T. and Giguere, P. A.: Hydrogen peroxide and its analogues. 2. Phase equilibrium in the system hydrogen peroxide water, Canad. J. Chem., 29, 123–132, doi:10.1139/v51-016, 1951.

ACPD

11, 26815–26848, 2011

The adsorption of peroxynitric acid on ice between 230 K and 253 K

T. Ulrich et al.

Gaffney, J. S. and Senum, G. I.: ?, in: Gas-liquid chemistry of natural waters, edited by: Newman, L., Brookhaven National Laboratory, 5-1–5-7, 1984.

Gierczak, T., Jimenez, E., Riffault, V., Burkholder, J. B., and Ravishankara, A. R.: Thermal decomposition of HO_2NO_2 (peroxynitric acid, PNA): Rate coefficient and determination of the enthalpy of formation, J. Phys. Chem. A, 109, 586–596, doi:10.1021/jp046632f, 2005.

Grannas, A. M., Jones, A. E., Dibb, J., Ammann, M., Anastasio, C., Beine, H. J., Bergin, M., Bottenheim, J., Boxe, C. S., Carver, G., Chen, G., Crawford, J. H., Domine, F., Frey, M. M., Guzman, M. I., Heard, D. E., Helmig, D., Hoffmann, M. R., Honrath, R. E., Huey, L. G., Hutterli, M., Jacobi, H. W., Klan, P., Lefer, B., McConnell, J., Plane, J., Sander, R., Savarino, J., Shepson, P. B., Simpson, W. R., Sodeau, J. R., von Glasow, R., Weller, R., Wolff, E. W., and Zhu, T.: An overview of snow photochemistry: evidence, mechanisms and impacts, Atmos. Chem. Phys., 7, 4329–4373, doi:10.5194/acp-7-4329-2007, 2007.

Guimbaud, C., Bartels-Rausch, T., and Ammann, M.: An atmospheric pressure chemical ionization mass spectrometer (APCI-MS) combined with a chromatographic technique to measure the adsorption enthalpy of acetone on ice, Int. J. Mass. Spectrom., 226, 279–290, doi:10.1016/S1387-3806(03)00019-8, 2003.

Heland, J., Kleffmann, J., Kurtenbach, R., and Wiesen, P.: A new instrument to measure gaseous nitrous acid (HONO) in the atmosphere, Environ. Sci. Technol., 35, 3207–3212, doi:10.1021/es000303t, 2001.

Hoffmann, M. R. and Jacob, D. J.: Kinetics and mechanisms of the catalytic oxidation of dissolved sulfur dioxide in aqueous solution: An application to nighttime fog water chemistry, in: SO_2, NO and NO_2 oxidation mechanisms: Atmospheric considerations, edited by: Calvert, J. G., Butterworth Publishers, Bosten, MA, USA, 101–172, 1984.

Huey, L. G.: Measurement of trace atmospheric species by chemical ionization mass spectrometry: Speciation of reactive nitrogen and future directions, Mass. Spectrom. Rev., 26, 166–184, doi:10.1002/mas.20118, 2007.

Huthwelker, T., Lamb, D., Baker, M., Swanson, B., and Peter, T.: Uptake of SO_2 by polycrystalline water ice, J. Colloid Interf. Sci., 238, 147–159, doi:10.1006/jcis.2001.7507, 2001.

Huthwelker, T., Ammann, M., and Peter, T.: The uptake of acidic gases on ice, Chem. Rev., 106, 1375–1444, doi:10.1021/cr020506v, 2006.

Hwang, H. and Dasgupta, P. K.: Thermodynamics of the hydrogen-peroxide water-system, Environ. Sci. Technol., 19, 255–258, doi:10.1021/es00133a006, 1985.

Hynes, R. G., Fernandez, M. A., and Cox, R. A.: Uptake of HNO3 on water-ice and coadsorp-

ACPD
11, 26815–26848, 2011

The adsorption of peroxynitric acid on ice between 230 K and 253 K

T. Ulrich et al.

tion of HNO_3 and HCl in the temperature range 210–235 K, J. Geophys. Res.-Atmos., 107, 4797, doi:10.1029/2001JD001557, 2002.

Jimenez, E., Gierczak, T., Stark, H., Burkholder, J. B., and Ravishankara, A. R.: Reaction of OH with HO_2NO_2 (peroxynitric acid): Rate coefficients between 218 and 335 K and product yields at 298 K, J. Phys. Chem. A, 108, 1139–1149, doi:10.1021/jp0363489, 2004.

Kenley, R. A., Trevor, P. L., and Lan, B. Y.: Preparation and thermal-decomposition of pernitric acid ($HOONO_2$) in aqueous-media, J. Am. Chem. Soc., 103, 2203–2206, doi:10.1021/ja00399a012, 1981.

Kerbrat, M., Huthwelker, T., Bartels-Rausch, T., Gäggeler, H. W., and Ammann, M.: Co-adsorption of acetic acid and nitrous acid on ice, Phys. Chem. Chem. Phys., 12, 7194–7202, doi:10.1039/b924782c, 2010a.

Kerbrat, M., Huthwelker, T., Gäggeler, H. W., and Ammann, M.: Interaction of nitrous acid with polycrystalline ice: Adsorption on the surface and diffusion into the bulk, J. Phys. Chem. B, 114, 2208–2219, doi:10.1021/jp909535c, 2010b.

Kim, S., Huey, L. G., Stickel, R. E., Tanner, D. J., Crawford, J. H., Olson, J. R., Chen, G., Brune, W. H., Ren, X., Lesher, R., Wooldridge, P. J., Bertram, T. H., Perring, A., Cohen, R. C., Lefer, B. L., Shetter, R. E., Avery, M., Diskin, G., and Sokolik, I.: Measurement of HO_2NO_2 in the free troposphere during the intercontinental chemical transport experiment – North America 2004, J. Geophys. Res.-Atmos., 112, D12S01, doi:10.1029/2006JD007676, 2007.

Kleffmann, J., Heland, J., Kurtenbach, R., Lorzer, J., and Wiesen, P.: A new instrument (LOPAP) for the detection of nitrous acid (HONO), Environ. Science Pollut. Res., 48–54, 2002.

Knight, G., Ravishankara, A. R., and Burkholder, J. B.: UV absorption cross sections of HO_2NO_2 between 343 and 273 K, Phys. Chem. Chem. Phys., 4, 1432–1437, doi:10.1039/b108904h, 2002.

Krepelova, A., Newberg, J. T., Huthwelker, T., Bluhm, H., and Ammann, M.: The nature of nitrate at the ice surface studied by XPS and NEXAFS, Phys. Chem. Chem. Phys., 12, 8870–8880, doi:10.1039/c0cp00359j, 2010.

Lammel, G., Perner, D., and Warneck, P.: Decomposition of pernitric acid in aqueous-solution, J. Phys. Chem.-US, 94, 6141–6144, doi:10.1021/j100378a091, 1990.

Lelieveld, J. and Crutzen, P. J.: The role of clouds in tropospheric photochemistry, J. Atmos. Chem., 12, 229–267, doi:10.1007/BF00048075, 1991.

Li, Z. J., Friedl, R. R., Moore, S. B., and Sander, S. P.: Interaction of peroxynitric acid with solid

ACPD
11, 26815–26848, 2011

The adsorption of peroxynitric acid on ice between 230 K and 253 K

T. Ulrich et al.

H2O ice, J. Geophys. Res.-Atmos., 101, 6795–6802, doi:10.1029/96JD00065, 1996.
Liss, P. S. and Slater, P. G.: Flux of gases across air-sea interface, Nature, 247, 181–184, doi:10.1038/247181a0, 1974.
Longfellow, C. A., Imamura, T., Ravishankara, A. R., and Hanson, D. R.: HONO solubility and heterogeneous reactivity on sulfuric acid surfaces, J. Phys. Chem. A, 102, 3323–3332, doi:10.1021/jp9807120, 1998.
Marsh, A. R. W. and McElroy, W. J.: The dissociation-constant and Henry law constant of HCl in aqueous-solution, Atmos. Envrion., 19, 1075–1080, doi:10.1016/0004-6981(85)90192-1, 1985.
McNeill, V. F., Loerting, T., Geiger, F. M., Trout, B. L., and Molina, M. J.: Hydrogen chloride-induced surface disordering on ice, P. Natl. Acad. Sci. USA, 103, 9422–9427, doi:10.1073/pnas.0603494103, 2006.
Niki, H., Maker, P. D., Savage, C. M., and Breitenbach, L. P.: Fourier-transform IR spectroscopic observation of pernitric acid formed via HOO + NO_2 → $HOONO_2$, Chem. Phys. Lett., 45, 564–566, doi:10.1016/0009-2614(79)85027-7, 1977.
Popp, P. J., Gao, R. S., Marcy, T. P., Fahey, D. W., Hudson, P. K., Thompson, T. L., Karcher, B., Ridley, B. A., Weinheimer, A. J., Knapp, D. J., Montzka, D. D., Baumgardner, D., Garrett, T. J., Weinstock, E. M., Smith, J. B., Sayres, D. S., Pittman, J. V., Dhaniyala, S., Bui, T. P., and Mahoney, M. J.: Nitric acid uptake on subtropical cirrus cloud particles, J. Geophys. Res.-Atmos., 109, D06302, doi:10.1029/2003JD004255, 2004.
Possanzini, M., Dipalo, V., and Liberti, A.: Annular denuder method for determination of H_2O_2 in the ambient atmosphere, Sci. Total Environ., 77, 203–214, doi:10.1016/0048-9697(88)90056-3, 1988.
Pouvesle, N., Kippenberger, M., Schuster, G., and Crowley, J. N.: The interaction of H_2O_2 with ice surfaces between 203 and 233 K, Phys. Chem. Chem. Phys., 12, 15544–15550, doi:10.1039/c0cp01656j, 2010.
Regimbal, J. M. and Mozurkewich, M.: Peroxynitric acid decay mechanisms and kinetics at low pH, J. Phys. Chem. A, 101, 8822–8829, doi:10.1021/jp971908n, 1997.
Servant, J., Kouadio, G., Cros, B., and Delmas, R.: Carboxylic monoacids in the air of mayombe forest (Congo) – Role of the forest as a source or sink, J. Atmos. Chem., 12, 367–380, doi:10.1007/BF00114774, 1991.
Slusher, D. L., Pitteri, S. J., Haman, B. J., Tanner, D. J., and Huey, L. G.: A chemical ionization technique for measurement of pernitric acid in the upper troposphere and the polar boundary

ACPD
11, 26815–26848, 2011

The adsorption of peroxynitric acid on ice between 230 K and 253 K

T. Ulrich et al.

layer, Geophys. Res. Lett., 28, 3875–3878, doi:10.1029/2001GL013443, 2001.
Slusher, D. L., Huey, L. G., Tanner, D. J., Chen, G., Davis, D. D., Buhr, M., Nowak, J. B., Eisele, F. L., Kosciuch, E., Mauldin, R. L., Lefer, B. L., Shetter, R. E., and Dibb, J. E.: Measurements of pernitric acid at the South Pole during ISCAT 2000, Geophys. Res. Lett., 29, 2011, doi:10.1029/2002GL015703, 2002.
Slusher, D. L., Neff, W. D., Kim, S., Huey, L. G., Wang, Y., Zeng, T., Tanner, D. J., Blake, D. R., Beyersdorf, A., Lefer, B. L., Crawford, J. H., Eisele, F. L., Mauldin, R. L., Kosciuch, E., Buhr, M. P., Wallace, H. W., and Davis, D. D.: Atmospheric chemistry results from the ANTCI 2005 Antarctic plateau airborne study, J. Geophys. Res.-Atmos., 115, D07304, doi:10.1029/2009JD012605, 2010.
Sokolov, O., and Abbatt, J. P. D.: Adsorption to ice of n-alcohols (ethanol to 1-hexanol), acetic acid, and hexanal, J. Phys. Chem. A, 106, 775–782, doi:10.1021/jp013291m, 2002.
Symington, A., Cox, R. A., and Fernandez, M. A.: Uptake of organic acids on ice surfaces: Evidence for surface modification and hydrate formation, Z. Phys. Chem., 224, 1219–1245, doi:10.1524/zpch.2010.6149, 2010.
Thibert, E. and Dominé, F.: Thermodynamics and kinetics of the solid solution of HNO_3 in ice, J. Phys. Chem. B, 102, 4432–4439, doi:10.1021/jp980569a, 1998.
Ullerstam, M., Thornberry, T., and Abbatt, J. P. D.: Uptake of gas-phase nitric acid to ice at low partial pressures: evidence for unsaturated surface coverage, Faraday Discuss., 130, 211–226, doi:10.1039/b417418f, 2005.
Vlasenko, A., Huthwelker, T., Gaggeler, H. W., and Ammann, M.: Kinetics of the heterogeneous reaction of nitric acid with mineral dust particles: An aerosol flowtube study, Phys. Chem. Chem. Phys., 11, 7921–7930, doi:10.1039/b904290n, 2009.
von Hessberg, P., Pouvesle, N., Winkler, A. K., Schuster, G., and Crowley, J. N.: Interaction of formic and acetic acid with ice surfaces between 187 and 227 K. Investigation of single species- and competitive adsorption, Phys. Chem. Chem. Phys., 10, 2345–2355, doi:10.1039/b800831k, 2008.
Wilhelm, E., Battino, R., and Wilcock, R. J.: Low-pressure solubility of gases in liquid water, Chem. Rev., 77, 219–262, doi:10.1021/cr60306a003, 1977.
Yaws, C. L. and Yang, H.-C.: Henry's law constant for compound in water, Thermodynamic and Physical Property Data, edited by: Yaws, C. L., Gulf Publishing Company Houston, Texas, USA, 181–206, 1992.

ACPD
11, 26815–26848, 2011

The adsorption of peroxynitric acid on ice between 230 K and 253 K

T. Ulrich et al.

Table 1. Solubility, acidity ($p\,K_a$), and adsorption enthalpies (ΔH_{ads}). The solubility is given as molecular Henry constant at 298 K (H_{298}).

Species	H_{298} [M atm^{-1}] min	H_{298} [M atm^{-1}] max	$p\,K_a$	ΔH_{ads} [k mol^{-1}] min	ΔH_{ads} [k mol^{-1}] max
NO	–	–	–	−17.4[17]	−22.6[17]
NO_2	–	–	–	−21[17]	−23[17]
HONO	37[1]	50[2]	3.25	−32[17]	−45[18]
HNO_3	2.1×10^{5}[3]	2.6×10^{6}[4]	−1.37	−44[17]	−68[19]
HO_2NO_2	4×10^{3}[5]	1.2×10^{4}[6]	5.85	−59[20]	–
HCl	1.1[7]	1.5×10^{3}[8]	−7	–	–
SO_2	1.1[9]	1.4[10]	1.77	–	–
H_2O_2	6.9×10^{4}[11]	1.4×10^{5}[12]	11.6	−32[21]	–
HCOOH	9×10^{2}[13]	1.3×10^{4}[14]	3.7	−51[22]	–
CH_3COOH	8.3×10^{2}[13]	1×10^{4}[15]	4.76	−17.5[23]	−55[22]
CF_3COOH	8.9×10^{3}[16]	–	0.3	–	–

[1]: Durham et al. (1981), [2]: Becker et al. (1996), [3]: Lelieveld and Crutzen (1991), [4]: Chameides (1984), [5]: Amels et al. (1996), [6]: Regimbal and Mozurkewich (1997), [7]: Marsh and McElroy (1985), [8]: Chen et al. (1979), [9]: Liss and Slater (1974), [10]: Wilhelm et al. (1977), [11]: Hwang and Dasgupta (1985), [12]: Hoffmann and Jacob (1984), [13]: Yaws and Yang (1992), [14]: Servant et al. (1991), [15]: Gaffney and Senum (1984), [16]: Bowden et al. (1996), [17]: Bartels-Rausch et al. (2002), [18]: Kerbrat et al. (2010b), [19]: Thibert and Dominé (1998), [20]: This study (2011)[21]: Pouvesle et al. (2010), [22]: von Hessberg et al. (2008), [23]: Sokolov and Abbatt (2002).

ACPD
11, 26815–26848, 2011

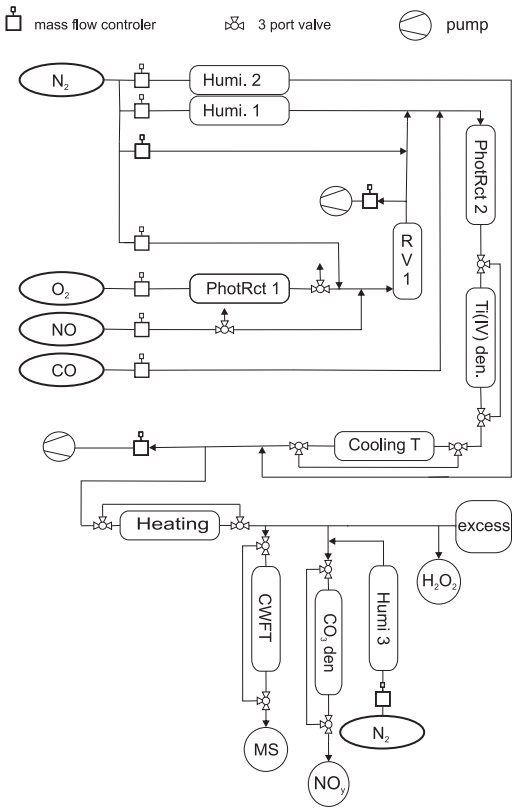

Fig. 1. Experimental setup consisting of a gas-phase synthesis, a purification step, the CWFT experiment, and the detection step. The H_2O_2 analyzer ("H_2O_2") was not integrated into the setup for all measurements.

ACPD
11, 26815–26848, 2011

The adsorption of peroxynitric acid on ice between 230 K and 253 K

T. Ulrich et al.

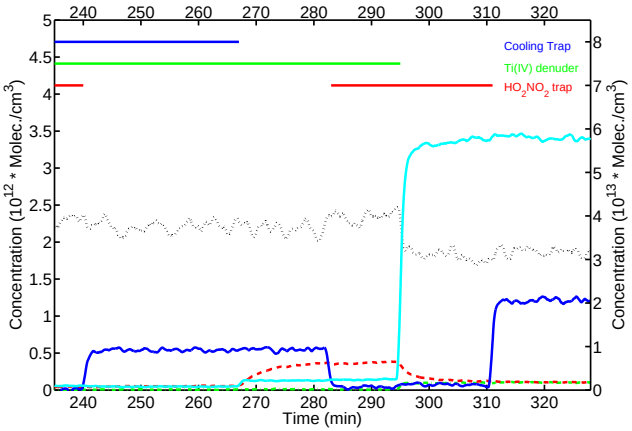

Fig. 2. Time traces of HO_2NO_2 (blue solid line, left axis) and the by-products NO_2 (black dotted line, left axis), HONO (green dash dotted line, left axis), HNO_3 (red dashed line, left axis), and H_2O_2 (turquoise solid line, right axis). Times at which traps were active are indicated by horizontal bars: Red: HO_2NO_2 trap (heating system), green: Ti(IV) denuder, blue: Cooling trap. Concentrations are given for the photolysis reactor, where the synthesis took place.

ACPD
11, 26815–26848, 2011

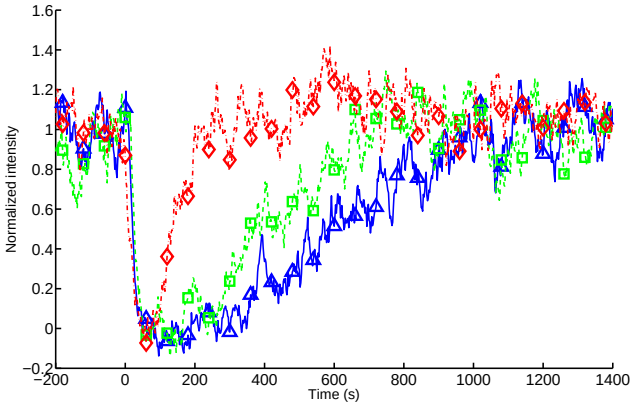

Fig. 3. Breakthrough curves of three CWFT adsorption experiments at 236 K (blue triangles), 240 K (green squares), and 250 K (red diamonds). The gas flow is led over the CWFT at time = 0 s. The variation in intensity at 250 K (t = 400–1000 s) is due to instrument fluctuations.

ACPD
11, 26815–26848, 2011

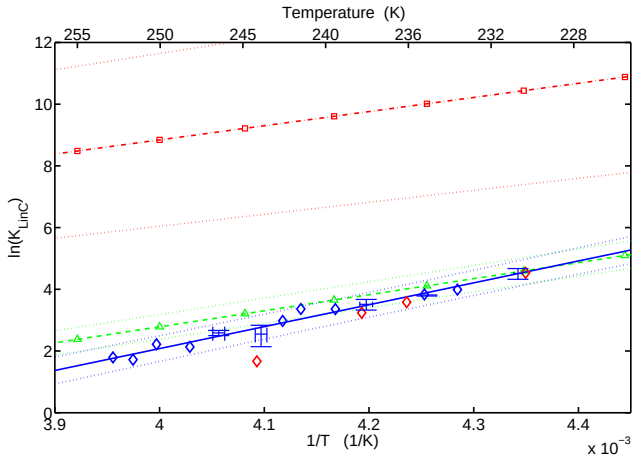

Fig. 4. Natural logarithm of K_{LinC} versus the inverse temperature for HO_2NO_2 (blue diamonds). If several data points were available mean values are plotted with an uncertainty of $1 \times \sigma$. The blue, dotted lines give the 95 % confidence bounds for the linear fit (blue solid line). The red diamonds indicate desorption experiments. The data are compared to the IUPAC recommendation (Crowley et al., 2010) for HONO (green, dashed line with triangles) and HNO_3 (red, dash-dotted line with squares). The dotted lines show the error for HONO and HNO_3 according to the IUPAC recommendation.

ACPD
11, 26815–26848, 2011

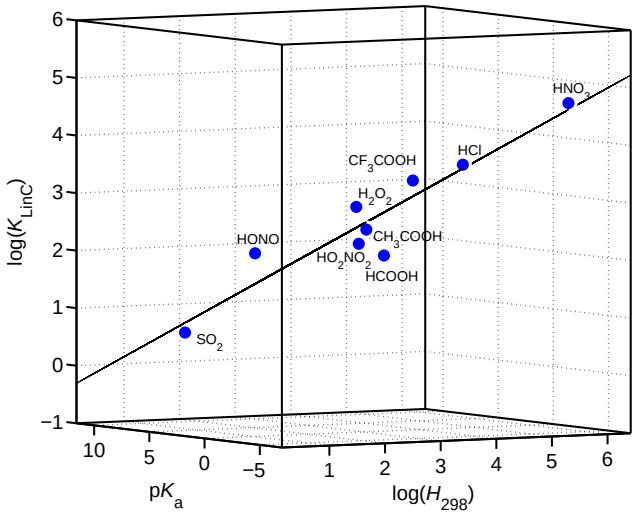

Fig. 5. Multiple linear regression with the input parameters acid dissociation constant ($p\,K_a$) and molecular Henry constant (H_{298} [M atm^{-1}]) versus the K_{LinC} [cm^{-1}] on ice at 228 K.

ACPD
11, 26815–26848, 2011

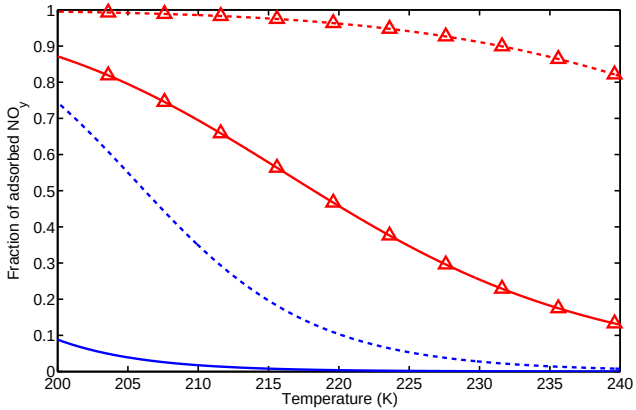

Fig. 6. Fraction of adsorbed HO_2NO_2 (blue line) and HNO_3 (red line, triangles) to cirrus clouds at temperatures of the upper troposphere. Solid lines represent clouds with a surface area density of 10^{-5} cm^{-1}, dashed lines represent clouds with a surface area density of 3×10^{-4} cm^{-1}.

ACPD
11, 26815–26848, 2011

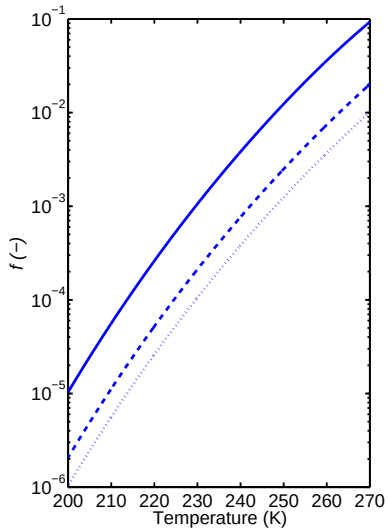

Fig. 7. Retention factor f versus temperature for three different surface area densities of snow: Solid line = 10 cm^{-1}, dashed line: 50 cm^{-1} and dotted line: 100 cm^{-1}.

ACPD
11, 26815–26848, 2011